# **ARTICLE**

# Effect of strand molecular length on mechanochemical transduction in elastomers probed with uniform force sensors†

Received 00th January 20xx, Accepted 00th January 20xx

DOI: 10.1039/x0xx00000x

Tetsu Ouchi,‡ac Wencong Wang,‡bc Brooke E. Silverstein,a Jeremiah A. Johnson\*bc and Stephen L. Craig\*ac

The mechanical properties of a polymer network reflect the collective behavior of all of the constituent strands within the network. These strands comprise a distribution of states, and a central question is how the deformation and tension experienced by a strand is influenced by strand length. Here, we address this question through the use of mechanophore force probes with discrete molecular weights. Probe strands, each bearing a mechanochromic spiropyran (SP), were prepared through an iterative synthetic strategy, providing uniform PDMS-functionalized SP force probes with molecular weights of 578, 1170, and 2356 g/mol. The probes were each doped (9 mM) into the same silicone elastomer matrix. Upon stretching, the materials change color, consistent with the expected conversion of SP to merocyanine (MC). The critical strain at which measurable mechanochromism is observed is correlated with the strain hardening of the matrix, but it is independent of the molecular length of the probe strand. When a network with activated strands is relaxed, the color dissipates, and the rate of decoloration varies as a function of the relaxing strain ( $\mathcal{E}_r$ ); faster decoloration occurs at lower  $\mathcal{E}_r$ . The dependence of decoloration rate on  $\mathcal{E}_r$  is taken to reflect the effect of residual tension in the once-activated strands on the reversion reaction of MC to SP, and the effect of that residual tension is indistinguishable across the three molecular lengths examined. The combination of discrete strand synthesis and mechanochromism provides a foundation to further test and develop molecular-based theories of elasticity and fracture in polymer networks.

## Introduction

The collective behavior of strands dictates the mechanical properties of a polymer network. 1-4 Thanks in part to the advent of single-molecule force spectroscopy/AFM,5-8 the mechanical behaviors of single molecules have been experimentally and theoretically well-characterized. Often, the various influences of the specific characteristics of a given strand (e.g., composition, length, orientation relative to applied strain, connectivity) within the collective, however, are hidden within the behavior of the ensemble. Elucidating the contributions of such molecular microstates will test and inform the evolution of theories of polymer elasticity and fracture, which might further lead to molecularly optimized mechanical properties. In addition, a better understanding of molecular structure-activity relationships in this area is likely to benefit emerging approaches to mechanically adaptive systems, especially in the field of mechanochemistry, where mechanophores induce changes in material properties such as stress-induced color changes,  $^{9-13}$  stress-strengthening,  $^{14-16}$  triggered degradation,  $^{17-19}$  and release of chemical cargo.  $^{20-24}$  For example, the elastically active strands within a polymer network generally comprise a range of molecular lengths between cross-links or entanglements ( $M_x$ , typically on the order of  $10^2$  to  $10^3$  g/mol), and an intuitive expectation is that shorter strands should serve as sites of focused tension, as a result of reaching their finite extensibility at smaller strains. The relationship between strand molecular length and mechanical response within a given network, therefore, represents an important factor that might guide the molecular design of mechanically active networks.  $^{25}$ 

Mechanophores represent powerful and promising tools for structure-activity relationship.9,26,27 investigating this Numerous examples of using mechanophores to probe fundamental questions of polymer network physical behavior have been reported. For example, Moore, Sottos, and coworkers applied spiropyran-based mechanophores polyacrylate-based<sup>11,28–31</sup> and polyurethane-based<sup>32,33</sup> networks to extensively investigate how the force transduction from macroscopic stress to the molecular tension felt by mechanophore probes is affected by various structural parameters, such as the positions of the mechanophore probes inside a polymer/filler composite<sup>34–38</sup> (i.e., matrix or interface) and orientation of chains.<sup>32</sup> Creton and co-workers incorporated 1,2-dioxetane-based mechanophore probes<sup>12</sup> into tough multi-networks to visualize where molecular chain scission occurs and the number of bonds that are broken during fracture.<sup>39</sup> Clough et al. used similar 1,2-dioxetane-based

<sup>&</sup>lt;sup>a</sup> Department of Chemistry, Duke University, Durham, North Carolina 27708, United States

b. Department of Chemistry, Massachusetts Institute of Technology, Cambridge, Massachusetts 02139, United States

<sup>&</sup>lt;sup>c</sup> NSF Center for the Chemistry of Molecularly Optimized Networks, Duke University, Durham, North Carolina 27708, United States

<sup>†</sup> Electronic Supplementary Information (ESI) available. See DOI: 10.1039/x0xx00000x

<sup>‡</sup> T. Ouchi and W. Wang contributed equally to this work

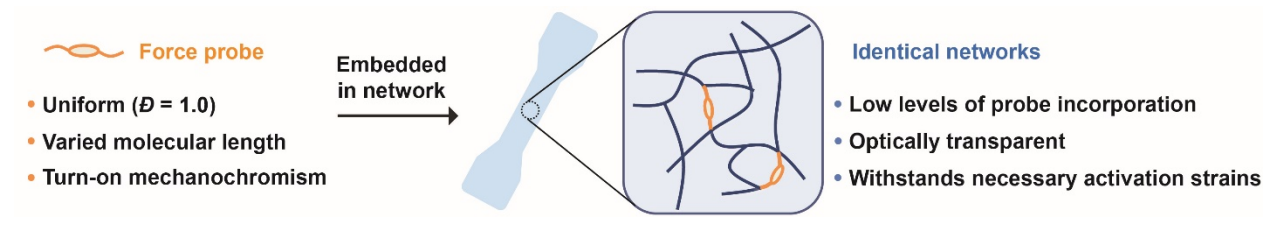


Fig. 1 The approach to analyze molecular behallor inside a polymer network

mechanophores to elucidate the contribution of chain scission to the Mullins effect in a silicone elastomer.<sup>40</sup> Recently, Lin et al. incorporated azobenzene-based mechanophores into a silicone elastomer and experimentally determined the average force that the azobenzene probe experiences as a function of the macroscopic strain of the network.<sup>41</sup> Building off of these and related advances, we sought to take advantage of the ability to probe strand state within a network to address a central question: to what extent does the tension felt by a strand with a network depend on the length of that particular strand, vs. the continuum behavior of the network to which it is tethered?

Our broad approach is summarized in Fig. 1. We envisioned mechanochromic probe strands of similar composition but different molecular lengths incorporated at low levels within the same polymer network continuum. By maintaining the same mechanophore reporter in all of the probe strands, any observed differences in probe strand response from one network to another could be attributed to the differences in the molecular length of the probe. We established the following criteria for an initial investigation: (i) a distinct, straindependent signal that can be detected at a level of probe strand incorporation that is too low to have a significant effect on network mechanical properties and topology; (ii) miscibility of the probe strand and other starting materials for network synthesis, to avoid challenges associated with the aggregation of mechanochromic molecules; (iii) truly uniform probe strands across a relevant range of strand length ( $M_x = 10^2-10^3$  g/mol,  $\theta$ = 1.0). The first criterion is satisfied through the use of the wellestablished mechanochromic force probe spiropyran, but the latter two criteria required synthetic method development.

The synthetic challenge began with the desire for uniform probes. A distribution of molecular weights is a necessary consequence of most abiological polymer synthesis methods, arising from the intrinsically stochastic nature of conventional step growth and addition polymerizations. This challenge has been creatively addressed through the development of solidphase synthesis,42-44 iterative exponential growth,45-48 and related approaches to discrete polymers.<sup>49–52</sup> To the best of our knowledge, however, these methods have yet to be applied to the synthesis of a series of mechanophore-incorporated strands of precise molecular weight. We therefore set out to synthesize discrete spiropyran-based probe strands that satisfy the above criteria. We chose the poly(dimethyl siloxane) (PDMS) elastomer Sylgard 184 as a testing matrix, since it is an industrially important and widely used elastomer that has also to be a robust platform for mechanochemistry, 10,13,53 including mechanochromism. We then used these SP-doped polymer networks to analyze the effects of strand molecular length on the mechanochemical reactivities and the tension experienced by the strand inside a common elastomeric matrix.

#### **Results and Discussion**

#### Bulk network effects and mechanochemical reactivities

Because we ultimately must compare networks that are made separately, we first evaluated how small variations in curing might influence molecular force transduction. For this purpose, we used commercially available silicone Sylgard 184 as the network matrix, due to its demonstrated utility as a platform for mechanophore activation and quantification, 10,13,53,54 and chose 1c (533 g/mol) for the force probe due to its proven activation inside the silicone elastomer.<sup>13</sup> Elastomer films with 1c (9 mM) were obtained through a platinum-catalyzed hydrosilylation reaction (Fig. 2), and differences in cured network structure and mechanical properties were created by intentional variation of the base to curing agent ratio of the two-component Sylgard kit (base:curing agent from 8:1 to 12:1, see Table S1). There is no SP aggregation observed in the X-ray scattering measurements (See SAXS, MAXS, and WAXS data in Fig. S2). The films are mechanically robust, and at large strains they exhibit the expected color change that is associated with the mechanically coupled conversion of SP to MC.

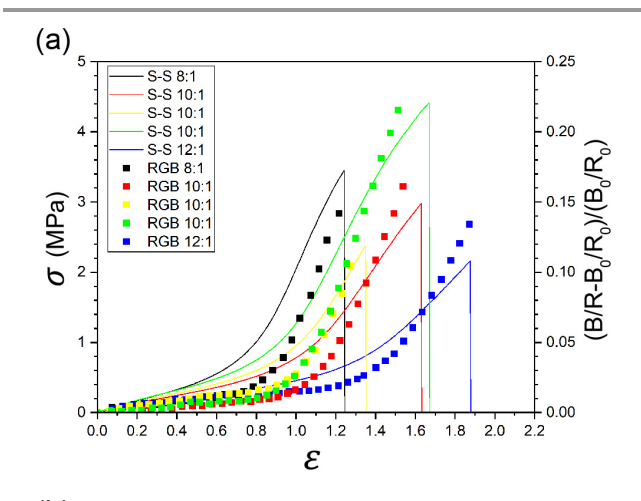
The mechanochemical response of the probe was quantified as a function of uniaxial tension (Fig. 3a). As expected, the initial modulus and onset strain of strain hardening ( $\varepsilon_{\text{SH}}$ , defined as the intersection of linear fits to the stress/strain curve before and after the nonlinear transition in the curve) vary slightly across replicates of the same 10:1 mixing ratio, and they vary even more when the component ratio is altered intentionally, with the 8:1 mixture being stiffer (with lower  $\varepsilon_{SH}$ ) and 12:1 being more compliant (higher  $\varepsilon_{SH}$ ). Simultaneously, the onset of mechanochromism ( $\varepsilon_c$ , defined as the intersection of linear fits to the RGB ratio curve before and after the nonlinear transition in the curve) was obtained from in-situ digital image color (RGB) analysis (Fig. 3a); the mechanochromism also changes from one film to another. The shifts in mechanochromism track with the shifts in  $\mathcal{E}_{SH}$  (Fig. 3a), a correlation that is borne out by plotting color as a function of normalized strain,  $\bar{\varepsilon} = \varepsilon / \varepsilon_{SH}$ . As shown in Fig. 3b, the mechanochromism across the five samples collapses to a common onset strain of approximately  $\bar{\varepsilon}$  = 1.1. The length of the probe stays the same, but the onset strain for mechanochromism varies, and that variation is correlated with the mechanical behavior of the surrounding network continuum. The surrounding polymer network, and in particular Journal Name ARTICLE

Fig. 2 Schematic of a PDMS elastomer incorporating SP probes

its strain hardening behavior, is one of the determining factors of force transduction.

#### Local strand effects and mechanochemical activation

We next sought to isolate the effects of strand length on force transduction. For a randomly coiled single macromolecule, the initial end-to-end distance  $(R_i)$  is proportional to the square root of the number of Kuhn lengths along its backbone  $(N^{1/2})$ , while the maximum length  $(R_{\rm max})$  is directly proportional to N. As such, the maximum extension to which an individual chain can be



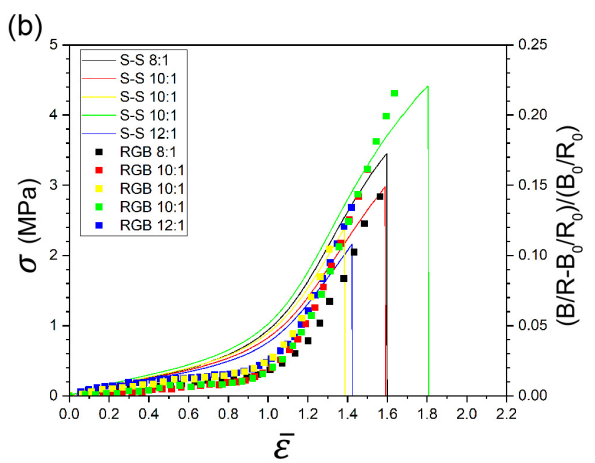


**Fig. 3** Stress-Strain curves and RGB ratio analysis of PDMS with different base and curing ratios: (a) before normalization and (b) after normalization. The ratios indicate base to curing agent ratios, and the three 10:1 samples are different batches.

stretched scales as  $\lambda_{\rm t} = R_{\rm max}/R_{\rm i} = N^{1/2}.^{55}$  If individual strands inside a polymer network deform affinely, strand length becomes an important factor in determining the onset of mechanochromism.

To analyze the effects of strand molecular length, we began by synthesizing discrete force probes that satisfy our criteria (mechanochromic, uniform, miscible) in the context of silicone elastomers. We adopted a strategy based on the iterative synthesis<sup>49</sup> of uniform poly(dimethyl siloxane)<sup>47</sup> from an SP core (Fig. 4a). The SP core was coupled to an  $\alpha$ , $\omega$ -chlorohydrido oligosiloxane chain extender through nucleophilic substitution of an SP hydroxyl with the chloride on the chain extender. Catalytic oxidation of the oligosilane hydride regenerated terminal hydroxyl groups for subsequent extension on both sides through a second and/or third cycle. This pathway allows for siloxane extension and is expected to help improve the miscibility of the probe strands and the silicone matrix. As this process was iterated with full control over the end-group functionality, the molecular weight grew linearly in a defined manner. Following zero, one, or three iterations, the strands were capped at the hydroxyl groups with allyl groups to give probe strands  $\mathbf{1}_0$ ,  $\mathbf{1}_1$ , and  $\mathbf{1}_3$ , respectively, where the subscript nrefers to the number of extension iterations involved in the synthesis of  $\mathbf{1}_n$ . Each of the three PDMS-based spiropyran (SP) force probe strands possess a single SP per chain, and the probes span discrete molecular weights of 578, 1170, and 2356 g/mol ( $\mathcal{D} = 1.0$ ) for  $\mathbf{1}_0$ ,  $\mathbf{1}_2$ , and  $\mathbf{1}_3$ , respectively.

The probe strands were characterized by NMR spectroscopy (Fig. S3-8), size exclusion chromatography (SEC, Fig. 4b), and MALDI-TOF mass spectrometry (Fig. 4c).  $^1$ H and  $^{13}$ C NMR show the signature peaks of SP in each probe strand, and peak integration in  $^1$ H NMR confirms the incorporation of one SP mechanophore per strand (Fig. S3-8). The SEC traces show sharp peaks with decreased retention times as the number of synthetic iterations increases, indicating the corresponding increase in molecular weight. Furthermore, MALDI-TOF mass spectra are dominated by a single peak at the expected mass/charge ratio of the strands, thus supporting their uniformity. We estimate the number of Kuhn lengths in the three strands to be N = 1.1, 2.6, and 5.7 for  $1_0$ ,  $1_2$ , and  $1_3$ , respectively (see Section G in ESI).  $^{55}$ 

We incorporated these discrete SP sensors into Sylgard 184 silicone elastomers (average molecular weight of 3,000 to 3,500 g/mol per elastically active strand with the functionality of 4) as

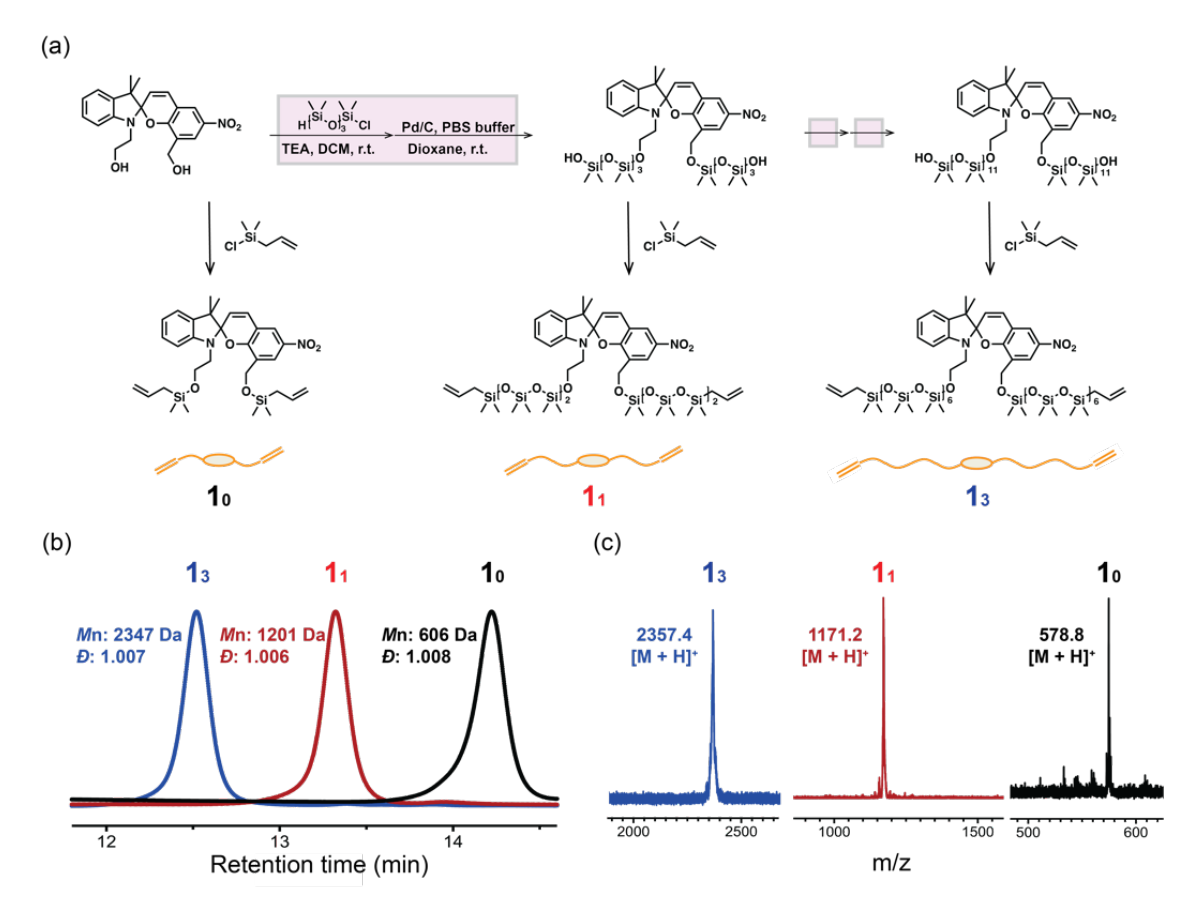


Fig. 4 (a) synthetic scheme for the SP probe strands with discrete molecular weights, (b) chloroform SEC traces of the SP probe strands, and (c) MALDI-TOF of the SP probe strands

shown in Fig. 2. Each of the SP probes  $\mathbf{1}_n$  were incorporated into the silicone matrix under identical conditions (9 mM probe, 10:1 base to curing agent) to produce elastomeric films through a platinum-catalyzed hydrosilylation. Here, the probe strands are miscible with the Sylgard kit, a feature we attribute to the use of siloxane extenders in the iterative synthetic approach. There is no SP aggregation observed in the X-ray scattering measurements (See Fig. S2 for SAXS, MAXS and WAXS data). Indeed, when polar triazoles were used to link the SP to PDMS handles, the probe strand was immiscible with the Sylgard matrix and good films were not obtained (results not shown).

The mechanical properties of the various films under uniaxial tension are consistent with well-formed silicone networks (Fig. 5a). The Young's moduli (E), ~1.0-1.2 MPa of the films with the various replicates fall within the range previously observed for replicates of the network doped with 1c. There might be some differences in the number of effective probe strands due to the different propensities of the three probes to form elastically inactive loops.<sup>56</sup> The presence of loops, however, only changes the magnitude mechanochromism and not the strain-dependent behavior examined here. Additionally, there is no evidence that the chain length of the SP probes has a significant effect on the mechanical properties of the network at this level of incorporation. When stretched by hand or scratched with a metal rod, all films develop a purple color that is clearly visible to the naked eye in the stretched/scratched regions,

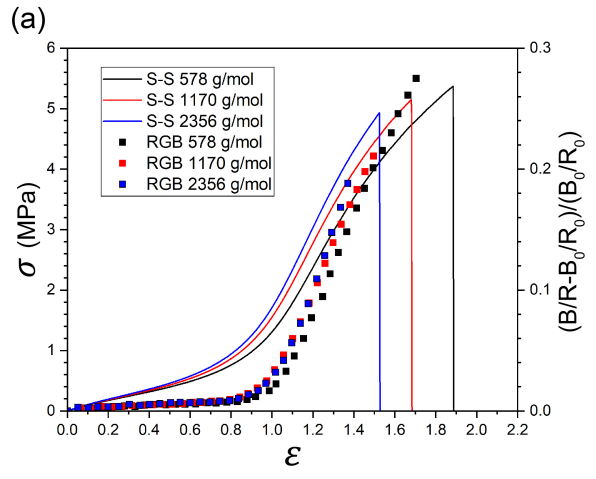
demonstrating successful mechanophore activation of SP to  $\ensuremath{\mathsf{MC}}.$ 

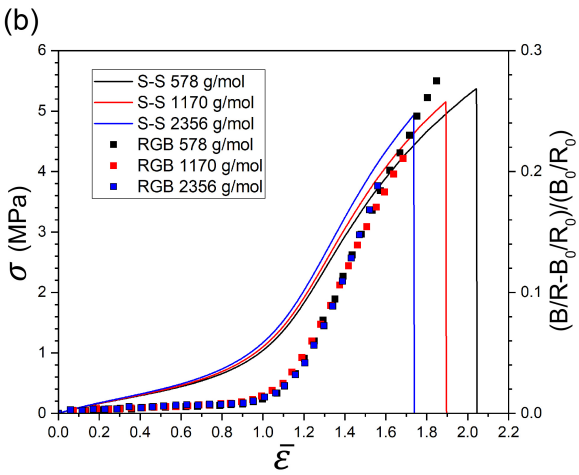
The mechanochromism of each film was tracked (Fig. 5a), and it again correlates with strain hardening behavior (Fig. 5b and c) in a manner that is indistinguishable from that observed in Fig. 3. A strong strand length dependency in the onset of the mechanochemical reaction ( $\varepsilon_c$ ) would be observed if the deformation of individual probe strands were affine, as would be expected from single molecule extension behavior. However, there is no obvious strand length dependency. The experimentally observed  $\varepsilon_c$  are 1.02, 0.98, and 1.01 for PDMS with  $\mathbf{1_0}$ ,  $\mathbf{1_1}$ , and  $\mathbf{1_3}$ , respectively, whereas an  $N^{1/2}$  dependence on  $\varepsilon_c$  would result in activation strains of ~2.2 for  $\mathbf{1_1}$  and 3.7 for  $\mathbf{1_3}$ , based on the  $\mathbf{1_0}$  benchmark. This trend is quite different from what one would expect from single molecule extension behavior and suggests non-affine deformation of individual strands inside the polymer networks.

## Strand length and mechanophore deactivation

Finally, we consider the mechanophores that are "turned on" when the strain exceeds  $\varepsilon_c$  and ask how those strands relax (i.e., how the mechanophores "turn back off" by reverting to SP from MC) as the strain applied to the network is reduced to values below  $\varepsilon_c$ . Specifically, the decoloration kinetics of the elastomers were analyzed as a function of time and normalized strain ( $\bar{\varepsilon} = \varepsilon/\varepsilon_{SH}$ ) to distinguish bulk network effects from local

Journal Name ARTICLE





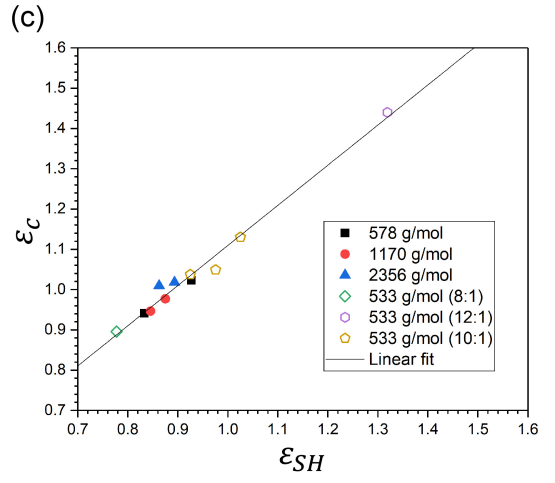


**Fig. 5** Stress-Strain curves and RGB ratio analysis: (a) before normalization and (b) after normalization, and (c) the onset strains for mechanochromism against those for strain hardening. R<sup>2</sup> of the linear fit is 0.98.

strand effects. Silicone elastomers were first stretched to  $\bar{\varepsilon}$  = 1.1 to induce force-activated MC states. After equilibrating for 30 min, the strain was lowered to a normalized relaxation strain  $(\overline{\varepsilon_r})$ , and the decoloration of the force-activated MC states back to SP was monitored as a function of the extent of relaxation (i.e., from  $\bar{\varepsilon}$  = 1.1 to  $\overline{\varepsilon_r}$  = 1.0 – 0.1).

To properly account for the effect of residual tension on decoloration rates, we first quantified the rates of MC reversion in unstrained films, by photochemically converting SP to MC and observing the rate at which color fades. The longest probe strands fade about 2 times more quickly than the shortest strands, a difference we attribute to small variations in local polarity that result from the tethers (Table S2). We therefore focus our analysis on the relative decoloration kinetics of a given probe as a function of  $\overline{\varepsilon_r}$ .

Two trends emerge from the data. First, lower  $\overline{\varepsilon_r}$ corresponds to faster decoloration (Fig. 6); just as the high tensions at large strains accelerate the conversion of SP to MC, the reversion of MC to SP is accelerated at lower strains. This strain-coupled effect is more obvious at  $\overline{\varepsilon_r}$  between 1.0 and 0.6. Below  $\overline{\varepsilon_r}$  = 0.6, the decoloration is effectively indistinguishable, indicating that the activated MCs experience negligible tension at these low strains. Second, as with the activation studies, the relative effect of tension on MC-to-SP reversion kinetics is indistinguishable across the series of probes. We quantified the strain dependence by normalizing the time axis of the decoloration at a given strain by  $t_{\rm rel}$  so that the data in each panel of Fig. 6 collapse onto a single master curve when color is plotted as a function of  $t/t_{\rm rel}$  (see Section I in ESI). For convenience, we convert  $t_{rel}$  to a relative rate constant  $k_{rel}$  given by equation (1):

$$k_{\rm rel} = k_0 t_{\rm rel} \tag{1}$$

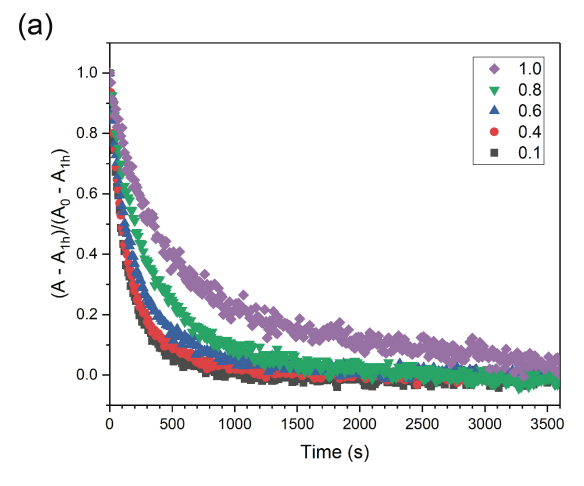
The normalized rate constants for decoloration are shown in Fig. 7a, confirming that residual tension affects the MC-to-SP reversion with no discernable influence from the probe strand length.

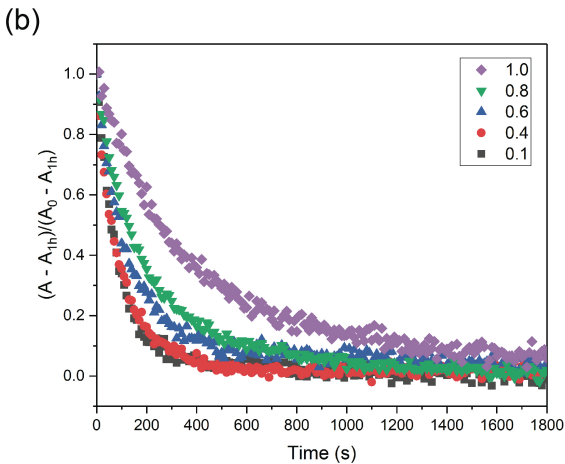
The magnitude of the average tension experienced in the strands can be estimated from the strain-dependent decoloration rates. At the molecular level, the relationship between rate and force of tension is often complex,  $^{57-59}$  but can often be estimated by assuming the simplest model of mechanochemical coupling (eq. 2), where  $k_{\rm B}$ , T, and  $\Delta x^{\ddagger}$  are Boltzmann constant, temperature, and the change in end-to-end distance between MC and transition states, respectively.

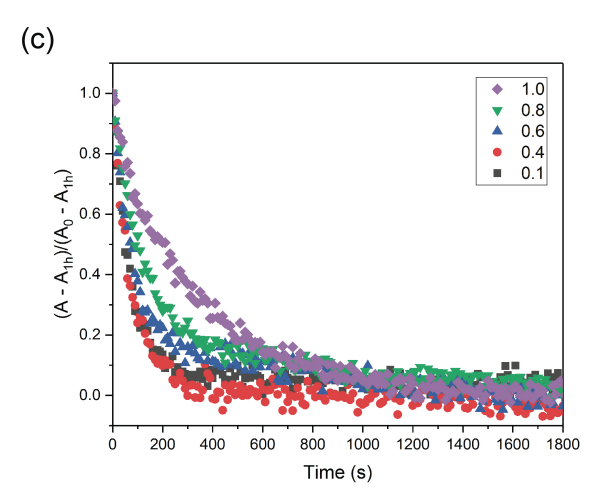
$$\langle F \rangle = (k_{\rm B}T/\Delta x^{\dagger})\ln(k_{\rm rel}/k_0)$$
 (2)

Within the constraints of this model, prior literature suggests a value of  $\Delta x^{\ddagger} = -2.13$  Å.  $^{60}$  Below  $\overline{\varepsilon_r} = 0.6$ , the average residual force calculated from eq. 1 and 2 is negligible, but increases from a few pN at  $\overline{\varepsilon_r} = 0.6$  to  $^{\sim}25$  pN at  $\overline{\varepsilon_r} = 1.0$  (Fig. 7b). Most importantly, the change in activated strand tension upon relaxing the network, like the strain-induced activation itself, is independent of strand length.

In addition to the primary observation regarding the (lack of) dependence on strand length, it is worth comparing the average tension per strand inferred here to that reported previously by Lin et al. for the cis-to-trans isomerization of a short azobenzene (AB) derivative ( $M_n \sim 400 \, \text{g/mol}$ , comparable to  $\mathbf{1}_0$ ) similarly embedded in Sylgard 184. In the AB system, there is no mechanical pre-activation; instead the rate of AB isomerization was fit to a two-state model that treated the AB derivatives as being either under negligible tension or being part of a subset of strands that experience measurable effects of tension akin to those explored here. The characteristic

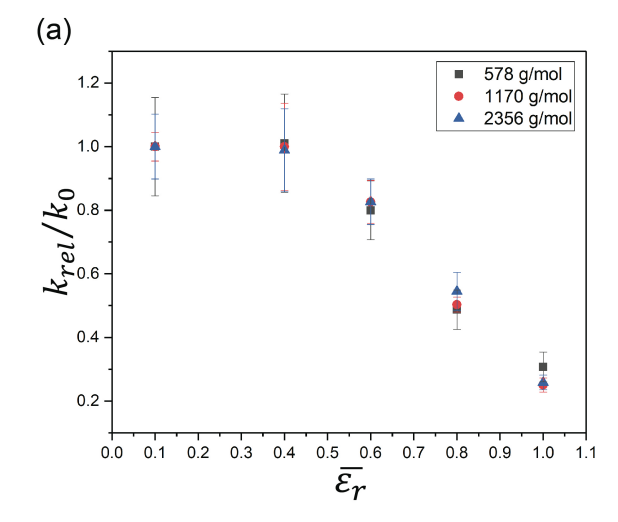






**Fig. 6** The relaxation kinetics of force activated MC back to SP states at each  $\bar{\varepsilon_{r'}}$ : (a) 578 g/mol, (b) 1170 g/mol, and (c) 2356 g/mol. The absorbance values are normalized as  $(A-A_{1h})/(A_0-A_{1h})$  for comparison.

residual forces acting on the SP probes at high normalized strain (e.g., ~25 pN at  $\overline{\epsilon_r}$  = 1.0 and  $\epsilon$  ~ 0.9) are similar to, but slightly lower than, those inferred previously from the AB kinetics at similar strain (~40 pN). Differences in the magnitude of tension are expected, as the populations of strands being probed in the two studies are not identical. For example, the design of the present study does not include the small subset of SP strands



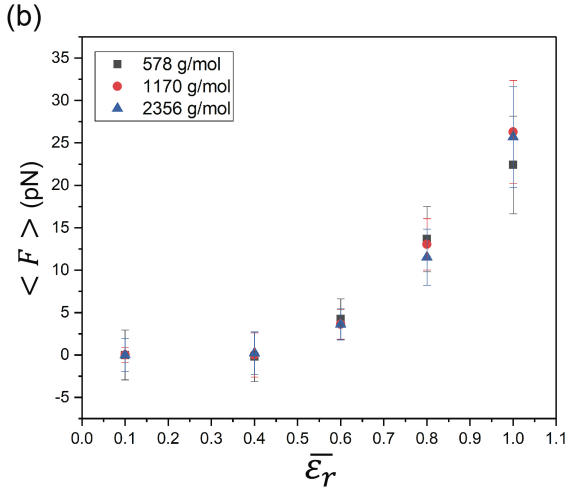


Fig. 7 (a) Ratios of reaction constants and (b) calculated average forces of preactivated probe strands as a function of relaxation strain and strand molecular weight.

under highest tension that do not revert back to MC; no such exclusion is intrinsic to the design in the previous work of Lin et al.

#### **Conclusions**

The use of discrete force probes of varied contour length provides insight into the behavior of specific sets of initial microstates within the canonical ensemble of a silicone elastomer. Polymer networks comprise a complex mixture of local strand lengths and topological connections, the details of which might vary greatly from one network to another in ways that influence the transduction of force among strands. The methods employed here using discrete force probes represent what we perceive to be a rich set of opportunities to use the increased precision afforded by contemporary synthetic methods to tease apart the contributions of specific structural microstates to the ensemble behavior of networks. We expect that these types of studies will help inform future molecularly based structure activity relationships and comprehensive physical models of network properties, including descriptions of

Journal Name ARTICLE

tension distribution and fracture behavior that have so far been the sole province of simulation.  $^{61,62}\,$ 

For the specific components studied here, the observations indicate that the bulk behavior of the network dominates mechanophore response to the exclusion of local strand length. On a fundamental level, the results cannot be interpreted through the lens of affine deformation of an individual strand. Rather, the macroscopic stress-strain curve, and especially the onset of strain-hardening, is the key correlant of molecular tension in overstressed strands. On a practical level, the results suggest a reasonable tolerance for strand length when embedding mechanophores. Such freedom in design might be useful in improving the compatibility of mechanophore and matrix, or in addressing the challenges of low mechanophore activation<sup>9,40,63</sup> by incorporating multiple mechanophores (including multiple types of mechanophores) into a single strand.<sup>64</sup> To that end, the Sylgard 184 matrix employed here is a commercially important and widely used elastomer that has be robust platform to а for covalent mechanochemistry. 10,13,33 As such, the findings should be applicable to other mechanically responsive systems.

Finally, we speculate as to the limits of the generality of the present observations. Due to synthetic feasibility, the probe strands employed here are shorter than the average strand in the network ( $N_{\rm avg} \simeq 8$  - 9), but we hypothesize that different behavior would be observed if the probe strand is (much) longer than the effective strand. For example, in the extreme, a strand with infinitely long molecular length should feel almost negligible force, even as the network around it is stretched to the point of strain hardening. This and other questions of molecular structure in polymer networks, including the effect of junction functionality and network topology, provide rich opportunities for future investigation.

#### Data availability

The experimental procedures and supporting data for this article have been included in the ESI.†

#### **Author contributions**

T.O., W.W., J.A.J., and S.L.C. conceived the project. T.O., W.W., J.A.J., and S.L.C designed the experiments. T.O. and B.E.S. performed the syntheses and structural characterization of the SP diol derivatives. W.W. conducted the synthesis and structural characterization of the SP probes with uniform molecular weights. T.O. synthesized PDMS elastomers with the SP probes and characterized their structures. T.O. conducted the tensile tests, image capturing, and reaction kinetics tests, and analyzed the data. T.O., W.W., J.A.J., and S.L.C. discussed the results. J.A.J. and S.L.C. provided the funding. T.O., W.W., J.A.J., and S.L.C. wrote the manuscript.

‡ T. Ouchi and W. Wang contributed equally to this work.

#### Conflicts of interest

There are no conflicts to declare.

# **Acknowledgements**

This material is based upon work supported by the National Science Foundation through the Center for the Chemistry of Molecularly Optimized Networks, under Grant No. CHE-2116298. The authors thank Dr. Liel Sapir for discussion and Dr. P. Silinski for assistance with the mass spectrometry.

#### **Notes and references**

- 1 M. Zhong, R. Wang, K. Kawamoto, B. D. Olsen and J. A. Johnson, *Science*, 2016, **353**, 1264–1268.
- 2 C. Creton and M. Ciccotti, *Reports Prog. Phys.*, 2016, **79**, 46601.
- 3 C. Creton, Macromolecules, 2017, **50**, 8297–8316.
- 4 S. Panyukov, Polymers, , DOI:10.3390/POLYM12040767.
- 5 G. Binning and C. F. Quate, *Handb. Phys. Med. Biol.*, 1986, **56**, 930–933.
- 6 A. Janshoff, M. Neitzert, Y. Oberdörfer and H. Fuchs, *Angew. Chemie Int. Ed.*, 2000, **39**, 3212–3237.
- 7 W. Zhang and X. Zhang, *Prog. Polym. Sci.*, 2003, **28**, 1271–1295.
- 8 H. J. Butt, B. Cappella and M. Kappl, *Surf. Sci. Rep.*, 2005, **59**, 1–152.
- 9 N. Deneke, M. L. Rencheck and C. S. Davis, *Soft Matter*, 2020, **16**, 6230–6252.
- 10 Y. Lin, M. H. Barbee, C. C. Chang and S. L. Craig, *J. Am. Chem. Soc.*, 2018, **140**, 15969–15975.
- 11 D. A. Davis, A. Hamilton, J. Yang, L. D. Cremar, D. Van Gough, S. L. Potisek, M. T. Ong, P. V. Braun, T. J. Martínez, S. R. White, J. S. Moore and N. R. Sottos, *Nature*, 2009, **459**, 68–72.
- 12 Y. Chen, A. J. H. Spiering, S. Karthikeyan, G. W. M. Peters, E. W. Meijer and R. P. Sijbesma, *Nat. Chem.*, 2012, **4**, 559–562.
- 13 G. R. Gossweiler, G. B. Hewage, G. Soriano, Q. Wang, G. W. Welshofer, X. Zhao and S. L. Craig, *ACS Macro Lett.*, 2014, **3**, 216–219.
- 14 T. Matsuda, R. Kawakami, R. Namba, T. Nakajima and J. P. Gong, *Science*, 2019, **363**, 504–508.
- 15 A. L. B. Ramirez, Z. S. Kean, J. A. Orlicki, M. Champhekar, S. M. Elsakr, W. E. Krause and S. L. Craig, *Nat. Chem.*, 2013, **5**, 757–761. 16 J. Wang, I. Piskun and S. L. Craig, *ACS Macro Lett.*, 2015, **4**, 834–837.
- 17 Y. Lin, T. B. Kouznetsova and S. L. Craig, *J. Am. Chem. Soc.*, 2020, **142**, 2105–2109.
- 18 Y. Lin, T. B. Kouznetsova, C. C. Chang and S. L. Craig, *Nat. Commun.*, 2020, **11**, 1–9.
- 19 T. G. Hsu, J. Zhou, H. W. Su, B. R. Schrage, C. J. Ziegler and J. Wang, *J. Am. Chem. Soc.*, 2020, **142**, 2100–2104.
- 20 P. B. Jayathilaka, T. G. Molley, Y. Huang, M. S. Islam, M. R. Buche, M. N. Silberstein, J. J. Kruzic and K. A. Kilian, *Chem. Commun.*, 2021, **57**, 8484–8487.
- 21 M. B. Larsen and A. J. Boydston, *J. Am. Chem. Soc.*, 2013, **135**, 8189–8192.
- 22 M. B. Larsen and A. J. Boydston, *J. Am. Chem. Soc.*, 2014, **136**, 1276–1279.
- 23 X. Hu, T. Zeng, C. C. Husic and M. J. Robb, *J. Am. Chem. Soc.*, 2019, **141**, 15018–15023.
- 24 Y. Sun, W. J. Neary, Z. P. Burke, H. Qian, L. Zhu and J. S. Moore, *J. Am. Chem. Soc.*, 2022, **144**, 1125–1129.
- 25 V. Sorichetti, A. Ninarello, J. M. Ruiz-Franco, V. Hugouvieux, W. Kob, E. Zaccarelli and L. Rovigatti, *Macromolecules*, 2021, **54**, 3769–3779.

- 26 Z. Xia, V. D. Alphonse, D. B. Trigg, T. P. Harrigan, J. M. Paulson, Q. T. Luong, E. P. Lloyd, M. H. Barbee and S. L. Craig, *Molecules*, , DOI:10.3390/molecules24030542.
- 27 M. Li, Q. Zhang, Y. N. Zhou and S. Zhu, *Prog. Polym. Sci.*, 2018, **79**, 26–39.
- 28 C. M. Kingsbury, P. A. May, D. A. Davis, S. R. White, J. S. Moore and N. R. Sottos, *J. Mater. Chem.*, 2011, **21**, 8381–8388.
- 29 Y. L. Loo, R. L. Willett, K. W. Baldwin and J. a. Rogers, *J. Am. Chem. Soc.*, 2002, **124**, 7654–7655.
- 30 M. N. Silberstein, K. Min, L. D. Cremar, C. M. Degen, T. J. Martinez, N. R. Aluru, S. R. White and N. R. Sottos, *J. Appl. Phys.*, , DOI:10.1063/1.4812581.
- 31 M. N. Silberstein, L. D. Cremar, B. A. Beiermann, S. B. Kramer, T. J. Martinez, S. R. White and N. R. Sottos, *J. Mech. Phys. Solids*, 2014, **63**, 141–153.
- 32 C. K. Lee, B. A. Beiermann, M. N. Silberstein, J. Wang, J. S. Moore, N. R. Sottos and P. V. Braun, *Macromolecules*, 2013, **46**, 3746–3752.
- 33 T. A. Kim, B. A. Beiermann, S. R. White and N. R. Sottos, *ACS Macro Lett.*, 2016, **5**, 1312–1316.
- 34 T. A. Kim, C. Lamuta, H. Kim, C. Leal and N. R. Sottos, *Adv. Sci.*, DOI:10.1002/advs.201903464.
- 35 T. Kosuge, K. Imato, R. Goseki and H. Otsuka, *Macromolecules*, 2016, **49**, 5903–5911.
- 36 Y. Zhang, E. Lund, G. R. Gossweiler, B. Lee, Z. Niu, C. Khripin, E. Munch, M. Couty and S. L. Craig, *Macromol. Rapid Commun.*, 2021, **42**, 1–7.
- 37 J. Sung, M. J. Robb, S. R. White, J. S. Moore and N. R. Sottos, *J. Am. Chem. Soc.*, 2018, **140**, 5000–5003.
- 38 J. W. Woodcock, R. Beams, C. S. Davis, N. Chen, S. J. Stranick, D. U. Shah, F. Vollrath and J. W. Gilman, *Adv. Mater. Interfaces*, 2017, **4**, 1–5.
- 39 E. Ducrot, Y. Chen, M. Bulters, R. P. Sijbesma and C. Creton, *Science*, 2014, **344**, 186–189.
- 40 J. M. Clough, C. Creton, S. L. Craig and R. P. Sijbesma, *Adv. Funct. Mater.*, 2016, **26**, 9063–9074.
- 41 Y. Lin, H. R. Hansen, W. J. Brittain and S. L. Craig, *J. Phys. Chem. B*, 2019, **123**, 8492–8498.
- 42 R. B. Merrifield, J. Am. Chem. Soc., 1963, 85, 2149-2154.
- 43 L. Hartmann, Macromol. Chem. Phys., 2011, 212, 8-13.
- 44 S. Huang and J. M. Tour, *J. Am. Chem. Soc.*, 1999, **121**, 4908–4909.
- 45 J. M. Schumm, Jeffry S.; Pearson. D. L.; Tour, *Angew. Chem. Int. Ed.*
- 46 J. C. Barnes, D. J. C. Ehrlich, A. X. Gao, F. A. Leibfarth, Y. Jiang, E. Zhou, T. F. Jamison and J. A. Johnson, *Nat. Chem.*, 2015, **7**, 810–815.
- 47 B. Van Genabeek, B. F. M. De Waal, M. M. J. Gosens, L. M. Pitet, A. R. A. Palmans and E. W. Meijer, *J. Am. Chem. Soc.*, 2016, **138**, 4210–4218.
- 48 Z. Huang, J. Zhao, Z. Wang, F. Meng, K. Ding, X. Pan, N. Zhou, X. Li, Z. Zhang and X. Zhu, *Angew. Chemie Int. Ed.*, 2017, **56**, 13612–13617.
- 49 S. C. Solleder, R. V. Schneider, K. S. Wetzel, A. C. Boukis and M. A. R. Meier, *Macromol. Rapid Commun.*, 2017, **38**, 1–45.
- 50 T. T. Trinh, C. Laure and J. F. Lutz, *Macromol. Chem. Phys.*, 2015, **216**, 1498–1506.
- 51 J. F. Lutz, M. Ouchi and M. Sawamoto, *Science*, 2013, **341**, 1238149.
- 52 M. A. R. Meier and C. Barner-Kowollik, *Adv. Mater.*, 2019, **31**, 1–5.
- 53 M. H. Barbee, K. Mondal, J. Z. Deng, V. Bharambe, T. V. Neumann, J. J. Adams, N. Boechler, M. D. Dickey and S. L. Craig, *ACS Appl. Mater. Interfaces*, 2018, **10**, 29918–29924.
- 54 T. A. Kim, M. J. Robb, J. S. Moore, S. R. White and N. R. Sottos, *Macromolecules*, 2018, **51**, 9177–9183.
- 55 M. Rubinstein and R. H. Colby, *POLYMER PHYSICS*, OXFORD UNIVERITY PRESS, 2003.

- 56 J. Wang, R. Wang, Y. Gu, A. Sourakov, B. D. Olsen and J. A. Johnson, *Chem. Sci.*, 2019, **10**, 5332–5337.
- 57 S. Akbulatov and R. Boulatov, *ChemPhysChem*, 2017, **18**, 1422–1450.
- 58 R. T. O'Neill and R. Boulatov, Synlett, 2022, 33, 851-862.
- 59 S. Akbulatov, Y. Tian, Z. Huang, T. J. Kucharski, Q. Z. Yang and R. Boulatov, *Science*, 2017, **357**, 299–303.
- 60 G. R. Gossweiler, T. B. Kouznetsova and S. L. Craig, *J. Am. Chem. Soc.*, 2015, **137**, 6148–6151.
- 61 R. Adhikari and D. E. Makarov, J. Phys. Chem. B, 2017, **121**, 2359–2365.
- 62 Y. Higuchi, K. Saito, T. Sakai, J. P. Gong and M. Kubo, *Macromolecules*, 2018, **51**, 3075–3087.
- 63 Y. Lin, T. B. Kouznetsova and S. L. Craig, *J. Am. Chem. Soc.*, 2020, **142**, 99–103.
- 64 B. H. Bowser and S. L. Craig, *Polym. Chem.*, 2018, **9**, 3583–3593.